Structure of Turbulent Sonic Underexpanded Free Jets

S. G. Chuech,* M.-C. Lai,† and G. M. Faeth‡
University of Michigan, Ann Arbor, Michigan

Turbulent mixing in adapted and weakly underexpanded (underexpansion ratios less than 1.4) round jets, involving fully developed pipe flows injected into still air, was studied experimentally. Measurements included mean and fluctuating concentrations and mean static pressures using laser-induced iodine flourescence and mean and fluctuating streamwise velocities using laser Doppler anemometry. Predictions were used to help interpret the measurements and to initiate evaluation of methods for analyzing these processes. The predictions were based on k-ϵ turbulence models, including a proposed extension to treat compressibility effects at high convection Mach numbers. In conjunction with other measurements, the results show that the near-field region of underexpanded jets is influenced by compressibility, which tends to reduce turbulent mixing rates at high convective Mach numbers, and high turbulence levels at the jet exit, which tends to increase turbulent mixing rates. Predictions based on effective-adapted-jet exit conditions yielded reasonably good estimates of mixing levels near the exit of underexpanded jets for both fully developed and slug flow jet exit conditions; however, such methods provide no information concerning the near-field region containing the shock waves. Predictions based on solution of parabolized Navier-Stokes governing equations, using the SCIPVIS algorithm, were encouraging for slug flow exit conditions, but this approach must be extended to treat fully developed flow at the jet exit.

Nomenclature

a = acceleration of gravity
C_μ = constant in turbulence model
d = jet exit diameter
f = mixture fraction
Fr = Froude number
k = turbulence kinetic energy
K = compressibility correction
M = Mach number
M_c = convective Mach number
p = static pressure
r = radial distance
u = streamwise velocity
x = axial distance
ϵ = rate of dissipation of turbulence kinetic energy
μ_t = turbulent viscosity
ν = kinematic viscosity

Subscripts

c = centerline quantity
e = jet exit condition
∞ = ambient condition

Superscripts

$(\bar{})(\bar{})'$ = time-averaged mean and root-mean-squared fluctuating quantity

Introduction

TURBULENT underexpanded free jets are an important fundamental flow, involving interactions between supersonic shock-wave-containing compressible flow and turbulent mixing. These flows also have a variety of practical applications, e.g., exhaust plumes of propulsion systems, breaks and vents in high-pressure systems, oil and gas well blowouts, stable injection of gases into liquids, and nuclear reactor pressure suppression systems, among others. Motivated by these considerations, one of the simplest of these flows was examined during the present investigation, namely, sonic injection of a turbulent round underexpanded air jet into still air. In order to complement available results for slug flow at the jet exit and to highlight interactions between turbulence and compressibility effects, the present measurements were limited to fully developed pipe flows at the injector exit. Flow properties also were predicted, using a typical k-ϵ turbulence model that had been calibrated for turbulent round jets, in order both to assist interpretation of the measurements and to initiate evaluation of methods for analyzing these processes.

Past investigations of underexpanded jets generally have used nozzles, yielding nearly slug flow conditions and low turbulence intensities at the jet exit. Adamson and Nicholls,[1] Crist et al.,[2] Davidor and Penner,[3] Addy,[4] and Ewan and Moody[5] studied the shock wave pattern near the jet exit. They found that at low underexpansion ratios (defined as the ratio between the jet exit and ambient static pressures) pressure equilibrium involved repetitive oblique shock cells, which eventually decayed into a conventional constant-pressure jet once the mixing layers at the edge of the shock-containing region reached the jet axis. For underexpansion ratios greater than 2–3, however, the first shock cells contained normal shock waves (Mach disks). The nozzle geometry was found to influence Mach disk properties: this was attributed to distortion of the sonic line.[4]

Measurements of the structure of underexpanded jets are relatively limited, due to difficulties caused by varying static pressures, high velocities, and shock waves. Measurements in the near-field shock-containing region generally have been limited to mean static pressures using probes, e.g., Seiner and Norum,[6,7] for flows generated by converging-diverging nozzles. More recently, Birch et al.[8,9] used hot-film anemometry and gas chromatography to measure mean velocities and concentrations in underexpanded jets; however, problems due to the formation of shock waves from the probes limited these measurements to the far-field, constant-pressure portion of the flow. Ewan and Moody[5] measured velocities in underex-

Received Nov. 19, 1987.

*Predoctoral Scholar, Department of Aerospace Engineering.
†Research Fellow, Department of Aerospace Engineering; currently Assistant Professor of Mechanical Engineering, Wayne State University, Detroit, MI.
‡Professor, Department of Aerospace Engineering. Fellow AIAA.

panded jets using laser Doppler anemometry, but well-known problems of the response of seeding particles to the rapid changes of velocities across shock waves limited their most reliable results to the constant-pressure region as well.

There have been several recent attempts to analyze underexpanded jets. Vatsa et al.[10] and Dash and co-workers[11-13] analyzed the pressure equilibration process using parabolized Navier-Stokes governing equations and a variety of turbulence models. Vatsa et al.[10] treated turbulence using an algebraic eddy viscosity model, finding encouraging agreement with measurements for weakly underexpanded jets. Dash and co-workers[11-13] examined the performance of several higher-order turbulence models: variants of k-ϵ models due to Launder et al.,[14] an empirical extension of these methods that allows for compressibility effects in high speed flows due to Dash et al.,[15] and the k-W model of Spalding.[16] Predictions were compared with the probe measurements of Seiner and Norum[6,7] for underexpanded jets and Eggers[17] for an adapted Mach 2.2 jet. On the whole, the comparison between predictions and measurements was encouraging, particularly for the k-W approach. This behavior is somewhat unexpected since the measurements of Seiner and Norum[6,7] and Eggers[17] involve high convective Mach numbers (ca. 0.9), whereas recent work indicates the compressibility effects should significantly reduce rates of turbulent mixing (see Bogdanoff[18] and Papamoschou and Roshko[19]). Dash and co-workers[11-13] point out, however, that there are significant uncertainties in these evaluations due to the limited data available to test the predictions of mixing for high-speed flows.

Due to the difficulties of exact treatment of the extermal expansion region of underexpanded jets, a number of approximate methods have been proposed. This involves avoiding detailed analysis of the near-field shock-containing region by seeking an equivalent adapted-jet initial condition to provide estimates of the structure of the constant-pressure portion of the flow. One approach involves approximating the flow by an equivalent fully expanded jet having the same stagnation pressure and enthalpy as the actual flow,[20,21] although several other methods have been proposed as well.[5,8,9,22] Evaluation of these methods, however, generally has been confined to streamwise positions far from the jet exit.

Limited experimental information, particularly measurements of mixing and turbulence properties, is clearly the major impediment for gaining a better understanding of turbulent underexpanded jets. Thus, the main objective of the present investigation was to complete nonintrusive measurements of the near-field shock-containing region of turbulent sonic underexpanded air jets in still air. Subsonic and sonic adapted jets also were considered to provide baseline information for evaluating experimental and theoretical methods extending to high-speed shock-free flows. As noted earlier, present measurements were limited to fully developed pipe flows at the jet exit, to complement the existing measurements for slug flow exit conditions. This introduces effects of turbulence in the core of the flow, which are known to influence near-field properties of low-speed jets. Detailed structure measurements were limited to weakly underexpanded jets, having underexpansion ratios less than 1.4; therefore, the flows involved only oblique shock waves, and convective Mach numbers were generally less than 0.6. As a result, effects of Mach disks were absent and effects of compressibility were small.

In order to help interpret the measurements and to initiate evaluation of methods for estimating flow properties, predictions also were made of flow structure. This involved use of a simplified k-ϵ turbulence model that was calibrated for constant- and variable-density round jets (for both slug and fully developed jet exit conditions) during earlier work in this laboratory.[23,24] A provisional extension of this approach to treat reduced turbulent mixing at high convective Mach numbers was also examined. Computations involved use of the approximate effective-adapted-jet methods, as well as the more complete parabolized Navier-Stokes method. In addition to present measurements, computations were compared with measurements in low-speed jets due to Birch et al.,[25] Shuen et al.,[24] Becker et al.,[26] and Wygnanski and Fiedler[27] and with the underexpanded jet measurements of Birch et al.[8,9] and Seiner and Norum[6,7]—the latter providing information on effects on compressibility at high convective Mach numbers for slug flow exit conditions.

The paper begins with a discussion of experimental and theoretical methods. Results for fully developed low-speed jets, fully developed sonic-adapted jets, slug flow underexpanded jets, and fully developed underexpanded jets then are considered in turn. The present discussion is brief; more details and a complete tabulation of data are provided by Chuech.[28]

Experimental Methods

Apparatus

The test apparatus was located in a room $6 \times 7.5 \times 4$ m high. Filtered air, having a dewpoint less than 240 K, was supplied to the jet from laboratory facilities. Airflow rates were controlled with a dome pressure regulator and metered with a standard critical-flow nozzle (Flow-Dyne Engineering, Inc., type NS16-7, with a calibration accuracy of 0.75%). The inlet temperature of the critical flow nozzle was monitored with a thermocouple.

The jet was horizontal. The inlet of the injector was fitted with a flow straightener, consisting of a 19 mm diam array of plastic straws, each having inside diameters of 6 mm and lengths of 75 mm. This was followed by a circular profile contraction (2.8:1 area ratio) to the jet passage. The jet passage was 9.5 mm in diameter and 50 diam long, to provide nearly fully developed pipe flow at the jet exit. Static pressures were monitored with four 500 μm diam taps (located 15, 45, 65, and 95 mm upstream from the jet exit), which were read with a bank of mercury manometers (each 1830 mm high). These measurements were extrapolated to find the static pressure at the jet exit.

Rigidly mounted optical diagnostics were used; therefore, the injector was traversed to measure properties at various points in the flow. The traverses were computer controlled with motor-driven Unislide Assemblies (Velmex, Inc., models B4018Q1J and B4021Q1J) having positioning accuracies of 5 μm. Four screw adjustments were used to control the height and angle of the jet.

Instrumentation

Measurements included flow visualization using continuous schlieren photography, mean and fluctuating streamwise velocities using laser Doppler anemometry (LDA), and mean and fluctuating concentrations and mean static pressures using laser-induced iodine fluorescence (LIF). Iodine vapor is relatively corrosive, even at low concentrations; therefore, components in contact with iodine were plexiglass (the injector), plastic, or brass—all of which have reasonably good corrosion resistance to iodine. The LDA and LIF systems are described in the following.

Velocity Measurements

Velocity measurements were carried out using a dual-beam forward-scatter LDA. Off-axis (25 deg) light collection was used, yielding a measuring volume having a diameter of 200 μm and a length of 460 μm. A Bragg cell frequency shifter (40 MHz) was used to control directional bias and ambiguity. Doppler signals were processed using a TSI 1990C burst counter with a 150 MHz maximum Doppler frequency. The flow was seeded using oil particles having average diameters of 500 nm. These particles had characteristic response frequencies of 30 kHz, which was adequate for measurements of subsonic and sonic flows, but could not resolve the rapid velocity changes encountered when passing through shock waves in the near-field region of the underexpanded jets. Seeding densities were less than 0.3 particles per measuring volume. In the sub-

sonic portions of the flow, the time between signals was less than integral time scales, yielding a low-burst-density/high-data-density signal. This allowed data reduction as time averages of the analog output of the burst counter signal processor without problems of velocity bias.

Bias errors and experimental uncertainties of the LDA measurements are discussed by Chuech.[28] Effects of gradient broadening were small, and experimental uncertainties were largely governed by finite sampling times. Estimated experimental uncertainties (95% confidence) were less than 10% for both mean and fluctuating velocities near the axis and were proportionally higher elsewhere. Measurements were repeatable within the range of the uncertainties.

Concentration Measurements

Laser-induced iodine fluorescence was used to measure mean and fluctuating concentrations, following Lai and Faeth.[29] This involved seeding the jet flow with iodine vapor. The LIF signal was induced using the 514.5 nm line (1700 mW of optical power) whose gain profile overlapped the iodine fluorescence transitions. A portion of the laser beam was used to monitor laser power and iodine seeding levels at the jet exit. The intensity of the beam passing through the measuring volume was also measured, so that effects of absorption on the beam power at the measuring location could be estimated. However, effects of absorption of the laser beam and reabsorption of fluorescence were small, since optical lengths were relatively short through the iodine-containing portions of the flow. The other two measurements allowed correction of raw data for variations of laser power and iodine seeding density. The LIF signal was observed off-axis (14 deg in the forward-scatter direction), yielding a cylindrical measuring volume having a diameter of 200 μm and a length of 1000 μm. The signal scattered to the detector included strong Rayleigh and Mie scattering signals at the laser line, along with fluorescence at longer wavelengths. The laser line signal was blocked with a long-pass optical filter to yield a signal proportional to the iodine concentration.[29] The bandwidth of the detector system was 5 MHz, which could resolve concentration fluctuations in the high-speed flows.

For present test conditions, based on the analysis of McDaniel,[30] the LIF signal was proportional to iodine concentration, inversely proportional to pressure due to quenching, and weakly varying with temperature (less than 11% change from the static temperature at sonic conditions to the lowest temperature experienced in the test flows).[28] As a result, concentrations were found by correcting the raw data for the static pressure at each point (using the mean static pressure measurements to be described next), since the effects of static pressure fluctuations were small. Measurements of power spectral densities yielded signal-to-noise ratios of ca. 1000, after optimization of detector parameters.

Errors and experimental uncertainties for the LIF measurements are discussed by Chuech.[28] Effects of gradient broadening were small; therefore, experimental uncertainties were largely governed by corrections for static pressure changes, finite sampling times, drift in experimental operating conditions and iodine seeding levels, and absorption of the laser beam and scattered fluorescence by iodine vapor. Due to these factors, experimental uncertainties (95% confidence) of mean concentrations were less than 10% when the static and ambient pressures were equal, increasing to less than 20% at the highest pressures where measurements were made. Errors in concentration fluctuations generally were higher, due to signal noise, but were generally less than 20%. Measurements were repeatable within the range of the uncertainties.

Static Pressure Measurements

Quenching of iodine LIF was used to measure mean static pressures by seeding the injected and ambient gas uniformly with iodine vapor, yielding an LIF signal that was inversely proportional to pressure for present test conditions.[28] This was accomplished by mounting the jet within a vented enclosure (710 mm in diameter and 810 mm long). The upstream end of the enclosure was sealed to the injector with a flexible bladder so that the injector could still be transversed. The arrangement of the LIF system was otherwise the same as for the concentration measurements.

Errors and experimental uncertainties of the static pressure measurements are discussed by Chuech.[28] These measurements were significantly gradient broadened across shock waves (ca. 1 mm) due to the finite size of the measuring volume; however, gradient broadening was small elsewhere. Experimental uncertainties were largely governed by effects of static temperature variations, discretization of the analog-digital (A/D) converter, and calibration accuracies. Exclusive of gradient broadening, experimental uncertainties (95% confidence) of the mean static pressure measurements are estimated to be less than 13% of the difference between static and ambient pressures.

Test Conditions

Test conditions for both present and related measurements are summarized in Table 1. Present measurements include subsonic and sonic adapted jets and sonic underexpanded jets having underexpansion ratios up to 1.37—all with jet exit con-

Table 1 Summary of test conditions[a]

Source	Injected gas	Diameter mm	Initial condition[b]	Under-expansion ratio	Mach no.	Convective Mach no.[c]	Reynolds no.[d]	Froude no.[e] $\times 10^6$
Adapted Jets								
Present	Air	9.5	FDF	1.00	0.30	0.16	57,300	11.5
Present	Air	9.5	FDF	1.00	1.00	0.48	268,000	1.04
Ref. 24	Air	10.9	FDF	1.00	0.10	0.05	22,000	104
Ref. 25	Methane	12.7	FDF	1.00	0.06	0.03	16,000	282
Ref. 26	Air	6.4	SF	1.00	0.38	0.19	54,000	3.68
Ref. 27	Air	26.4	SF	1.00	0.21	0.10	120,000	49.9
Underexpanded Jets								
Present	Air	9.5	FDF	1.20	1.00	0.54	321,600	1.04
Present	Air	9.5	FDF	1.37	1.00	0.58	367,200	1.04
Ref. 8	Natural gas	2.7	SF	1.90	1.00	0.77	163,000	0.15
Ref. 9	Air	2.7	SF	1.90	1.00	0.65	167,600	0.27
Ref. 7	Air	50.0	SF	1.45	2.00	0.94	8,000,000	1.87

[a]Injection into still air at normal temperature and pressure.
[b]FDF = fully developed flow; SF = slug flow.
[c]Maximum convective Mach number in flow, as defined in Ref. 19.
[d]$Re = u_e d/\nu_e$.
[e]$Fr = ad/u_e^2$.

ditions that approximate fully developed pipe flow. The convective Mach numbers of all present flows were all less than 0.6; therefore, effects of compressibility on turbulent mixing are expected to be relatively small, based on the results of Bogdanoff[18] and Papamoschou and Roshko.[19]

Results from other studies, summarized in Table 1, also were considered. This includes measurements of adapted low-speed jets from Shuen et al.,[24] Birch et al.,[25] Becker et al.,[26] and Wygnanski and Fiedler[27] and for underexpanded jets due to Birch et al.[8,9] and Seiner and Norum.[6,7] Except for Shuen et al.[24] which approximated fully-developed pipe flow, all these flows involved slug flow jet exit conditions. The jets considered by Birch et al.[8,9] and Seiner and Norum[6,7] involved convective Mach numbers greater than 0.6, where significant effects of compressibility on turbulent mixing are expected.[18,19]

All flows to be considered were reasonably turbulent, $Re > 10^4$. Those having significant effects of buoyancy (suggested by large Froude numbers), like Shuen et al.[24] and Birch et al.,[25] were injected vertically; therefore, axisymmetry was preserved for these flows as well.

Theoretical Methods

General Description

Computations were performed for the flows summarized in Table 1. Properties of adapted jets were found using the GENMIX algorithm due to Spalding,[31] while the properties of underexpanded jets were found using the parabolized Navier-Stokes approach, based on the SCIPVIS algorithm due to Dash et al.[11] Computations for the underexpanded jets also included use of the effective-adapted-jet approximation, with other aspects of these calculations similar to those for adapted jets.

Calculations were based on the following major assumptions: steady (in the mean) axisymmetric flow with no swirl; a still gaseous environment; either negligible effects of buoyancy or buoyancy forces aligned with the streamwise direction; either the boundary-layer approximations (adapted jets) or the approximations of parabolized Navier-Stokes analysis (underexpanded jets); ideal-gas mixture with constant specific heats; equal exchange coefficients of all species and heat; in cases where buoyancy is important, effects of buoyancy considered in the governing equations for only mean quantities; negligible effects of density fluctuations; and negligible effects of radiation.

Most of these assumptions are either conditions of the experiments or have been justified, and yielded acceptable results, in the past.[11-16,23,24] Neglecting effects of density fluctuations, however, is one of the most questionable assumptions and deserves further discussion. For the present adapted jets, static temperature changes are less than 20% with comparable levels of density changes, while regions where density changes are largest also have relatively low turbulence levels; therefore, density fluctuations are small throughout the flow and neglecting them introduces little error. Potential density fluctuations are greater for computations using the effective-adapted-jet approximations for underexpanded jets, but neglecting density fluctuations in these cases seems appropriate in view of the other approximations of this approach. Density fluctuations are potentially significant for underexpanded jets using the parabolized Navier-Stokes approach; however, the greatest departures of density from ambient values occur in regions where turbulence intensities are small; therefore, in keeping with past computations,[11-13] the assumption is adopted here as well. The main advantage is that this approximations provides a unified formulation for both the adapted and underexpanded jets.

Adapted Jets

The formulation for adapted jets follows earlier work in this laboratory,[23,24] and these sources, as well as Chuech,[28] should be consulted for the details. The original formulation was based on Favre averages for low-speed flows, using the conserved-scalar formalism and a k-ϵ-g turbulence model. Under present assumptions, the Favre and time averages are the same; however, effects of significant levels of kinetic energy must be considered when scalar properties are found. This was done following Dash et al.[11] to obtain an approach consistent with the parabolized Navier-Stokes calculations for the underexpanded jets, by solving an additional governing equation for conservation of stagnation enthalpy. This extension was evaluated using present measurements for the subsonic and sonic jets.

It is well known that turbulent mixing rates are reduced for supersonic compressible flows in comparison to subsonic flows.[11-15,18,19] Dash et al.[15] developed a compressibility correction to deal with this phenomenon; however, evaluation of this approach has not been very encouraging.[11-13] A somewhat different approach was examined during the present investigation as a provisional extension of the baseline k-ϵ turbulence model. This involved a correction to the expression for turbulent viscosity, similar to Dash et al.[15]; however, the correction was correlated in terms of the convective Mach number of the turbulent mixing layer as a whole. This choice was motivated by the recent findings of Bogdanoff[18] and Papamoschou and Roshko,[19] which suggest the importance of the convective Mach number for describing the mixing properties of high-speed turbulent flows.

The compressibility-corrected version of the k-ϵ turbulence model (denoted c.c. in the following) uses the following modified expression for the turbulent viscosity:

$$\mu_t = \bar{\rho} C_\mu K k^2/\epsilon \tag{1}$$

where K is the compressibility correction. The following correlation was used for K:

$$\begin{aligned} &K = 1.00, && M_c < 0.55 \\ &K = 2.03 - 1.87\, M_c, && 0.55 \le M_c \le 0.95 \\ &K = 0.25, && 0.95 > M_c \end{aligned} \tag{2}$$

where M_c is the convective Mach number of the mixing layer, found as described by Papamoschou and Roshko.[19] The form of Eq. (2) was established by plotting the ratio of compressible to incompressible mixing layer growth rates as a function of the convective Mach number, similar to Papamoschou and Roshko,[19] using measurements from Papamoschou and Roshko,[19] Maydew and Reed,[32] Sirieux and Solignac,[33] Birch and Eggers,[34] Brown and Roshko,[35] and Ikawa and Kubota.[36] All these results were obtained for constant-pressure mixing layers with low turbulence intensities in the undisturbed streams. Similar to the plot presented by Papamoschou and Roshko,[19] all these results correlated reasonably well, with little effect of compressibility for $M_c <$ ca. 0.5, a sharp transition for ca. $0.5 < M_c <$ ca. 1.0, and with mixing rates roughly 25% of incompressible mixing rates for $M_c >$ ca. 1.0—as reflected by the correlation of Eq. (2).

Initial conditions for the calculations were prescribed at the jet exit. Measurements indicated that mean and turbulence quantities for the present flows and those of Shuen et al.[24] closely approximated fully developed pipe flows. Thus, the mean velocity distribution was taken from Schlichting[37] and the distributions of k and ϵ were taken from Hinze[38] for fully developed pipe flow at the appropriate Reynolds number. Initial conditions for slug flows were estimated, similar to earlier work.[13,22,23]

The equations were solved using a modified version of the GENMIX algorithm due to Spalding.[31] The computational grid involved 33-99 cross-stream grid nodes, with streamwise step sizes no larger than 6% of the current flow width or 5% entrainment—whichever was smaller. Overall numerical accuracy was tested by halving all grid sizes for some typical conditions; this yielded changes of dependent variables less than 1% from the results reported here.

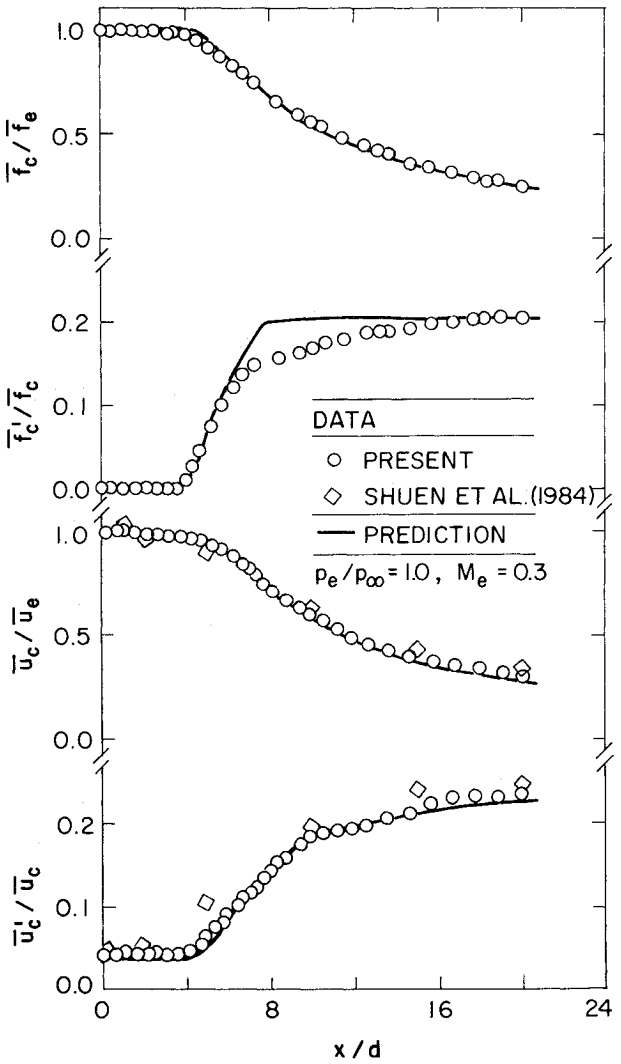

Fig. 1 Mean and fluctuating quantities along axis in subsonic jets.

Effective-Adapted-Jet Approximation

Aside from the specification of initial conditions, calculations for underexpanded jets using the effective-adapted-jet approximation were the same as for the adapted jets. Three effective-adapted-jet approximations were examined, as follows: 1) the divergent nozzle approach,[21,22] 2) the pseudo-diameter approach,[8] and 3) the momentum velocity approach.[22] All three methods gave nearly the same results for present conditions; therefore, only findings for the divergent nozzle approach will be illustrated in the following. This method is favored, since it at least preserves conservation of mass, momentum, and energy of the flow when the effective jet exit condition is prescribed, while the other methods do not.

The divergent nozzle approximation replaces the flow at the exit of an underexpanded jet with conditions that would result after isentropic expansion of the flow to the ambient pressure. No virtual origin was used—the new exit condition was applied at the actual location of the jet exit. The character of the flow for the effective effect condition also was taken to be the same as the actual flow, i.e., either fully developed pipe or slug flow.

Underexpanded Jets

Calculations for the parabolized Navier-Stokes approach used the SCIPVIS algorithm of Dash and co-workers.[11-13] The SCIPVIS algorithm was developed for analysis of propulsion systems, where turbulence levels at the jet exit are typically small. Thus, the algorithm separates the flowfield into an inviscid shock cell region along the axis near the injector exit, surrounded by mixing layers growing along the edge of the flow (with provision for treating the Mach disk mixing layer in the core of the flow, when it is present). Thus, only mean properties are required at the jet exit. This is a serious limitation for predictions of the present flows, since fully developed exit conditions, with significant levels of turbulence throughout the shock-containing region, cannot be treated exactly. Nevertheless, it is still useful to compare SCIPVIS predictions with present measurements in order to highlight potential effects of a strongly turbulent flow at the jet exit.

Specification of the computational grid and evaluation of numerical accuracy for the SCIPVIS calculations were the same as for the adapted jets. An additional difficulty with SCIPVIS calculations, noted by Dash and Wolf,[11] is that a still ambient environment cannot be computed directly; a coflow must be imposed to stabilize the solutions. It was found that even the lowest level of coflow influenced predictions; therefore, a series of calculations were carried out for various coflows and Richardson extrapolation was used to find results for a still ambient environment. Fortunately, the effect of coflow was regular, so that uncertainties introduced by the extrapolation are not felt to be large in comparison to other uncertainties of the predictions.[28]

Results and Discussion

Adapted Jets

Present measurements of mean and fluctuating concentrations and streamwise velocities along the axis of the subsonic jet are plotted in Fig. 1. Earlier measurements of Shuen et al.[24] as well as predictions also appear on the plot. All results appearing on the figure pertain to fully developed pipe flow at the jet exit. Predictions for both flows were virtually the same and are represented by a single line. The effects of compressibility were small for all calculations associated with the present measurements, with the baseline and compressibility-extended predictions being essentially the same; therefore, these versions will not be distinguished on the plots. The assumption of isotropic turbulence was used to estimate velocity fluctuations from the predictions, e.g., $\bar{u}'^2 = 2k/3$. If the usual level of anisotropy observed near the axis of fully developed turbulent jets was assumed instead[27] (e.g., $\bar{u}'^2 = k$), the predictions would be roughly 20% higher. The measurements are limited to the near-injector region, where the flow is still developing ($x/d \leq 20$); therefore, it is likely that actual levels of anisotropy are between these limits.

Present measurements of streamwise mean and fluctuating velocities agree with those of Shuen et al.[24] within the experimental uncertainties. This is consistent with the well-known weak dependence of flow properties on the Reynolds number of reasonably turbulent jets when plotted in the manner of Fig. 1. This is reflected by the predictions, which similarly show little difference between the two sets of experiments. Flow properties vary slowly with streamwise distance for $x/d < 4$, exhibiting a potential-core-like region near the jet exit. This region is substantially shorter than the potential core of low-speed jets having slug flow exit conditions, which normally extends to $x/d \sim 8$.[27] This behavior is due to faster mixing with the surroundings, promoted by the higher jet exit turbulence levels for the fully developed flows. Another effect of jet exit conditions is that concentration fluctuation intensities increase at a faster rate than velocity fluctuation intensities downstream of the potential-core-like region. This is caused by the fact that concentration fluctuations are formally zero at the jet exit, while the velocity fluctuations are rather large at the jet exit—representative of fully developed pipe flows.

Similar to past experience with the present turbulence model, for low-speed constant- and variable-density jets,[22-24] there is reasonably good agreement between the predictions and measurements illustrated in Fig. 1. In particular, the predictions provide a good estimate of the length of the potential-core-like region and the measured faster growth rate for con-

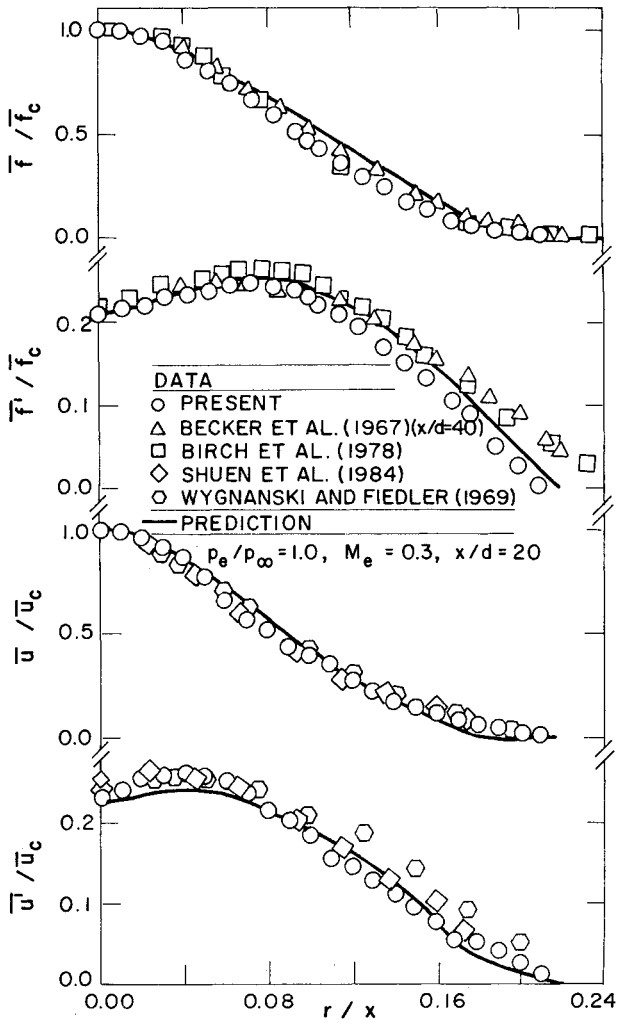

Fig. 2 Mean and fluctuating quantities in subsonic jets at $x/d = 20$.

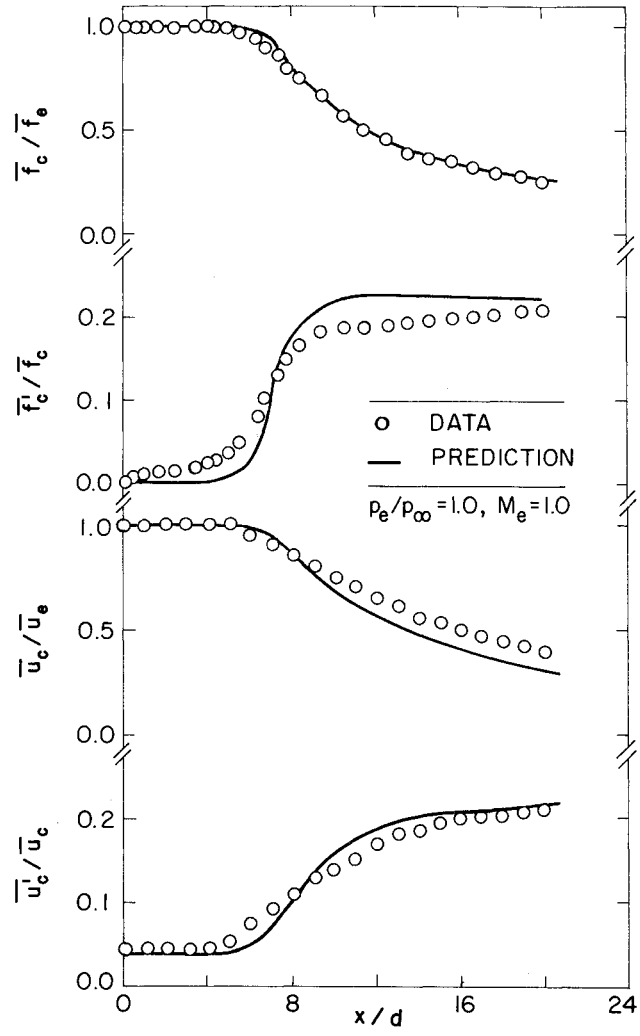

Fig. 3 Mean and fluctuating quantities along axis in the sonic jet.

centration intensities in comparison to velocity intensities downstream of this region. The largest discrepancy between predictions and measurements involves concentration intensities for $8 < x/d < 16$. Effects of gradient broadening of the measurements are relatively small in this region, suggesting difficulties with predictions. In particular, use of the boundary-layer approximation may be responsible for the error, since concentration fluctuations increase rapidly in the streamwise direction within this region, as noted earlier.

Flow properties in the subsonic jet, at $x/d = 20$, are illustrated in Fig. 2. Properties are plotted as a function of r/x, which is the similarity variable for fully developed turbulent jets,[27] so that the actual flow width can be seen. At this position, properties are relatively independent of initial conditions when normalized as in Fig. 2; therefore, several other measurements are plotted on the figure for comparison with present findings. Mean properties of all the measurements agree reasonably well with each other and with the predictions. The velocity fluctuation measurements of Shuen et al.,[24] also made with an LDA, similarly agree with present measurements and predictions. However, the velocity fluctuation measurements of Wygnanski and Fielder[27] are higher near the edge of the flow, probably due to difficulties in interpreting their hot-wire measurements for conditions where the turbulence intensities are high. The concentration fluctuation measurements of Becker et al.[26] and Birch et al.[25] also are higher than the present measurements near the edge of the flow. This is expected for the particle-scattering approach used by Becker et al.,[26] since shot noise increases the apparent concentration fluctuation levels and is difficult to control when particle concentrations are low. Birch et al.[25] use Raman scattering, where shot noise should not be a problem; thus, the reason for this discrepancy is not known.

On the whole, predictions and measurements in Fig. 2 agree within experimental uncertainties, which is typical of past experience with the present turbulence model for low-speed jets.[23,24] In particular, predictions represent absolute levels of velocity and concentration fluctuations at the axis and the different positions of the maxima of these properties reasonably well. Thus, the approach provides a useful baseline for extension to high-speed jets.

Measurements and predictions along the axis of the sonic jet are illustrated in Fig. 3. The potential-core-like region extends to roughly $x/d = 6$ for the sonic jet, in comparison to roughly $x/d = 4$ for the low-speed jet (cf. Figs. 1 and 3). This is caused by the increased initial density of the sonic jet, due to its lower static temperature, so that additional mixing with the surrounding gas is required in order to achieve the same scalar and dynamical state. However, other properties of the two flows are similar, including the faster growth rate of concentration intensitites than velocity intensities downstream of the potential-core-like region.

The comparison between predictions and measurements for the sonic jet is similar to the subsonic jet (cf. Figs. 1 and 3). The increased length of the potential-core-like region and the growth rate of velocity intensities are predicted reasonably well, while discrepancies are present for the more rapidly growing concentration intensities, similar to the subsonic jet.

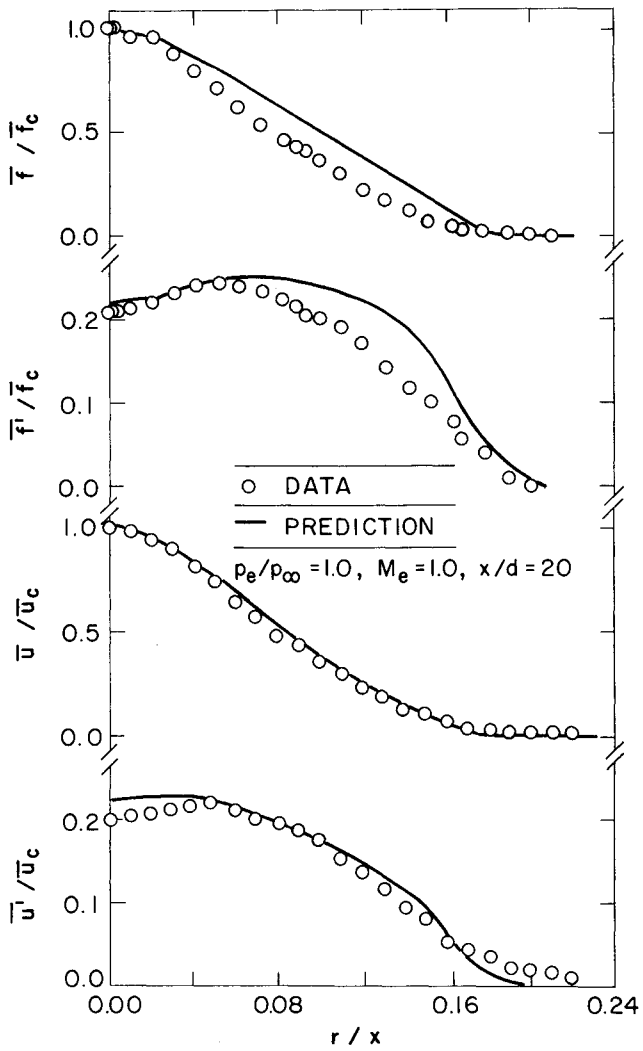

Fig. 4 Mean and fluctuating quantities in the sonic jet at $x/d = 20$.

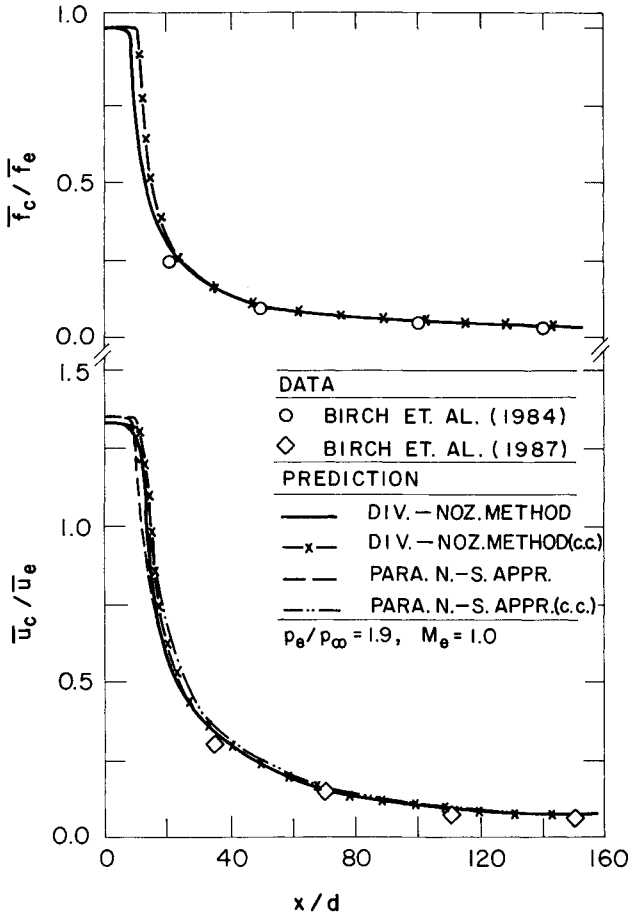

Fig. 5 Mean velocities and concentrations along axis in underexpanded jets (slug flow, $p_e/p_\infty = 1.9$, $M_e = 1.0$, from Refs. 8 and 9).

The present formulation has treated variable-density, low-speed jets successfully in the past,[23] and the highest convective Mach numbers of the flows considered in Figs. 1-3 are lower than the regime where compressibility effects are known to influence rates of turbulent mixing.[18,19] Therefore, this agreement is perhaps not surprising. The additional feature examined here, however, involves consideration of high-speed flows with density changes due to changes of velocity. The results illustrated in Fig. 3 suggest that these aspects of the formulation are performing satisfactorily.

Measurements and predictions of flow properties at $x/d = 20$ for the sonic jet are illustrated in Fig. 4. The fully developed flow region is being approached at this position and measured properties, as normalized in Fig. 4, are not very different from the low-speed jet. However, predictions are modified in the near-field region, due to effects of density changes. Thus, there are somewhat larger discrepancies between predictions and measurements in Fig. 4 than Fig. 2, although the differences are not large in comparison to experimental uncertainties.

Underexpanded Jets: Slug Flow

Underexpanded jets with slug flow jet exit conditions will be considered before examining the additional complications resulting from fully developed pipe flow at the jet exit. Measurements to be considered include those of Birch et al.[8,9] and Seiner and Norum.[6,7] Two jets were studied by Birch et al.: natural gas injected into still air to study mixing and air injected into still air to study velocity distributions. Convective Mach numbers for these flows are 0.77 and 0.65, while the measurements are limited to $x/d > 20$; therefore, the effects of compressibility are probably not large for these experiments. In contrast, the Seiner and Norum measurements were obtained near the jet exit, with a convective Mach number of 0.94, so that strong effects of compressibility should be present.[19]

Measurements and predictions for the jets considered by Birch et al.[8,9] are illustrated in Fig. 5. Measurements included mean concentrations along the axis for the methane jet and mean velocities along the axis for the air jet. Predictions based on the divergent nozzle approximation, with and without the compressibility correction, are illustrated for both jets. Parabolized Navier-Stokes predictions using the SCIPVIS algorithm, with and without the compressibility correction, are limited to the air jet. The SCIPVIS calculations give rapid mean velocity fluctuations in the shock-wave-containing region near the jet exit, which cannot be resolved on the scale of Fig. 5; therefore, only the averages of these mean velocity fluctuations along the axis are shown. Velocities computed using the divergent-nozzle approximation do not fluctuate and are plotted directly on the figure; these velocities are higher than the jet exit velocity due to the effective expansion process between the jet exit and ambient pressures.

All the mean velocity predictions illustrated in Fig. 5 agree reasonably well with each other and with the measurements. However, this evaluation is not very definitive since the measurements correspond to the slug flow exit conditions, which are appropriate for SCIPVIS; the convective Mach numbers are low so that compressibility should not have a large effect on mixing; and the measurements are far from the jet exit, reducing effects of errors in the near-field region. Use of the divergent nozzle approximation is similarly successful for mean

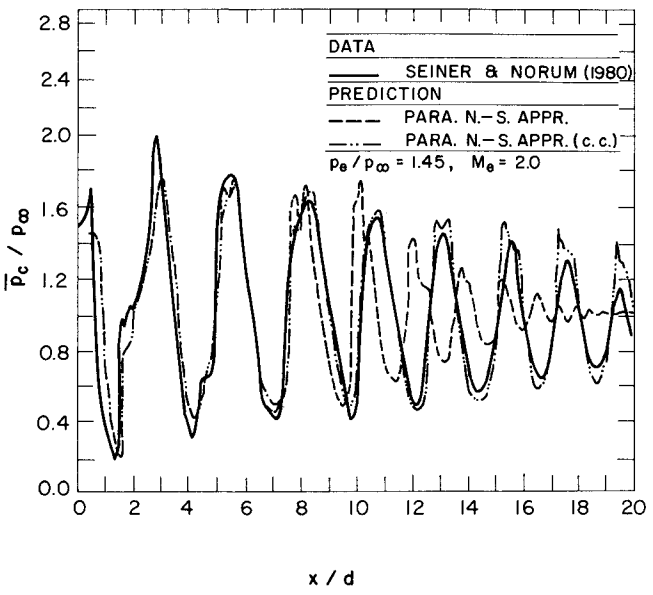

Fig. 6 Mean static pressures along axis in an underexpanded jet (slug flow, $p_e/p_\infty = 1.45$, $M_e = 2.0$, from Refs. 6 and 7).

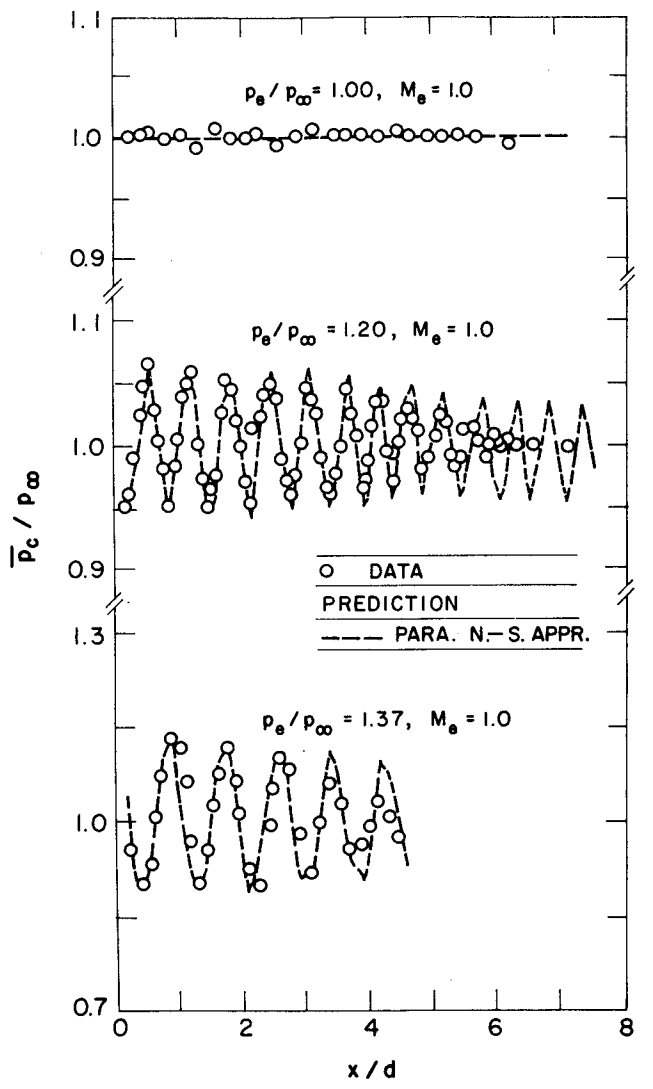

Fig. 7 Mean static pressures along axis in adapted and underexpanded jets.

concentrations along the axis, but with the same limitations. While the effects of compressibility are not large for the results illustrated in Fig. 5, they still can be seen in the predictions. The lower values of K for $M_c > 0.55$ cause the compressibility-corrected predictions to trail the baseline predictions, extending the length of the potential core region slightly.

The mean static pressure measurements along the axis of an underexpanded supersonic jet, due to Seiner and Norum,[6,7] are illustrated in Fig. 6. Predictions using the SCIPVIS algorithm, both with and without the compressibility correction, are also shown on the figure. Both predictions and measurements exhibit the decaying oscillatory static pressure variation caused by the interaction between the shock cells and the growing mixing layers near the edge of the flow in the near-field region. All predictions and the measurements agree quite well for the first few shock cells, where the flow is largely inviscid; similar behavior was observed by Dash et al.[12] using slightly different turbulence models. Farther downstream, however, predictions using the baseline turbulence model underestimate the wavelength of the pressure oscillations and overestimate their rate of decay in the streamwise direction. This is caused by overestimation of the rate of growth of the shear layers near the edge of the flow, which is reduced due to the high convective Mach number of this flow, 0.94. This is shown by the improved predictions of the compressibility-corrected version of the turbulence model, both with respect to the wavelength and amplitudes of the pressure oscillations far from the injector. These results suggest that the reduced rates of mixing for the Seiner and Norum[6,7] measurements are consistent with the constant-pressure high convective Mach number measurements used to develop the correlation of Eq. (2).

Underexpanded Jets: Fully Developed Flow

Predictions using the SCIPVIS algorithm and measurements of time-averaged mean static pressures along the axis of adapted and underexpanded jets for fully-developed jet exit conditions are illustrated in Fig. 7. Convective Mach numbers for these flows were small; therefore, predictions with or without the compressibility correction are nearly the same and only single prediction lines are shown. Measurements for the adapted jet exhibit a small but regular variation of static pressure near the jet exit, instead of the uniform mean static pressure field appropriate for an adapted jet. The pressure variation is comparable to experimental uncertainties; nevertheless, it was reproducible and suggests that the sonic adapted jet was actually slightly underexpanded. Velocity profiles near the jet exit exhibited slight acceleration effects, suggestive of underexpansion as well.[28] This difficulty was encountered since defining the sonic state is somewhat subjective when flow properties at the jet exit are not uniform.

The static pressure variations, illustrated in Fig. 7, correspond to the shock cell pattern observed on the schlieren photographs of the flow.[28] The amplitude of the pressure oscillations decreases and the frequency increases until the shock cell pattern disappears as the sonic line within the strong mixing layer near the edge of the flow reaches the axis. This process is completed by $x/d = 6$–7 for an underexpansion ratio of 1.20. The pressure field decays in a similar manner for a underexpansion ratio of 1.34; however, the full region of decay could not be observed due to the appearance of strong Mie scattering signals from the mixing layer. This difficulty was caused by vapor condensation, due to the lower static temperature levels in this flow.

Similar to the static pressure results for slug flow illustrated in Fig. 6, predictions for fully developed flow illustrated in Fig. 7 are in reasonably good agreement with measurements for the first few shock cells, where effects of turbulent mixing are small. Farther downstream, however, predictions overestimate the amplitude and wavelength of the pressure oscillations, yielding a longer shock-wave-containing region than measured. This behavior is opposite to the findings for slug

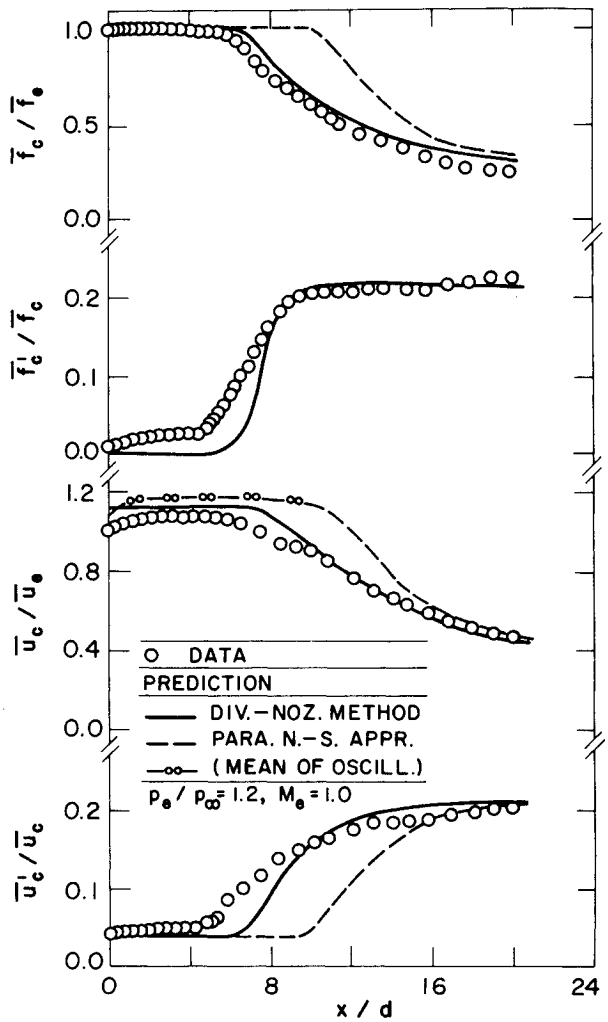

Fig. 8 Mean and fluctuating quantities along axis in an underexpanded jet.

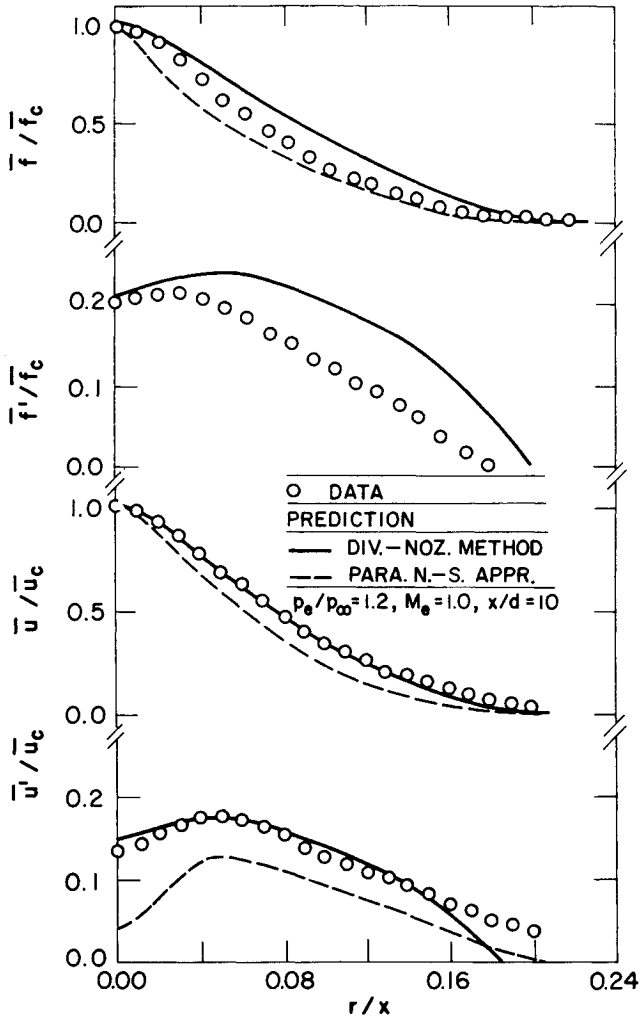

Fig. 9 Mean and fluctuating quantities in an underexpanded jet at $x/d = 10$.

flow jet exit conditions where the length of the shock-containing region was underestimated using the baseline turbulence model (cf. Figs. 6 and 7). The convective Mach numbers of the underexpanded fully developed flows are less than 0.6; therefore, compressibility effects are small, so that both baseline and compressibility-corrected predictions are the same in Fig. 7. Thus, the presence of a fully turbulent core flow, as opposed to the inviscid flow prescribed by the SCIPVIS algorithm, is mainly responsible for this behavior; e.g., with an adjacent turbulent flow, the strong mixing layer near the edge of the flow grows more rapidly, causing faster decay of the shock cell pattern. The same effect is responsible for the shorter length of the potential-core-like region for fully developed jet exit conditions, than for slug flow, for low-speed jets.

Measured mean and fluctuating concentrations and streamwise velocities along the axis of the jet having an underexpansion ratio of 1.2 are illustrated in Fig. 8. Predictions using both SCIPVIS and the divergent nozzle approximation are also illustrated on the figure. The length of the potential-core-like region for the underexpanded jet is similar to the sonic jet (cf. Figs. 3 and 8), which is somewhat surprising due to the vastly different core flow when shock cells are present. Measured mean velocities in the shock-containing region could not resolve the velocity changes across shock cells due to deficiencies in particle response. Thus, only values beyond the potential-core-like region are reliable.

As expected from the static pressure results, predictions using SCIPVIS overestimate the length of the potential-core-like region. This behavior is not due to an inviscid effect, e.g., the shift in position of the sonic line between slug flow and fully developed pipe flow jet exit conditions, since the SCIPVIS algorithm allows use of the actual initial mean velocity distribution at the jet exit. As noted earlier, faster growth of the strong mixing layer near the edge of the flow, due to the presence of the turbulent core, appears to be the most probable explanation for the differences between SCIPVIS predictions and measurements.

The predictions using the divergent nozzle approximation are in best agreement with measurements in Fig. 8. Although the divergent nozzle approach is somewhat ad hoc, it can account for effects of degree of flow development at jet exit and gave reasonably good results for other adapted and underexpanded jets. Thus, the improved agreement between the divergent nozzle predictions and the measurements is supportive of the importance of turbulence at the jet exit on the near-field properties of underexpanded jets. More exact treatment of this process is very challenging, since the interaction between the strong mixing layer and the turbulent core, which have different turbulence properties, must be considered in the presence of shock waves and effects of compressibility.

Measured flow properties at $x/d = 10$ and 20 appear in Figs. 9 and 10. Predictions using both the SCIPVIS algorithm and the divergent nozzle approximation also appear on the figure. The region considered is just downstream of the shock-wave-containing region, and the measured flow properties are similar to results for adapted jets when plotted in the manner of Figs. 9 and 10 (see Figs. 2 and 4). The divergent nozzle approximation gives respectable predictions, similar to its performance for adapted jets at the same locations, even though the shock-wave-containing region ends only slightly upstream

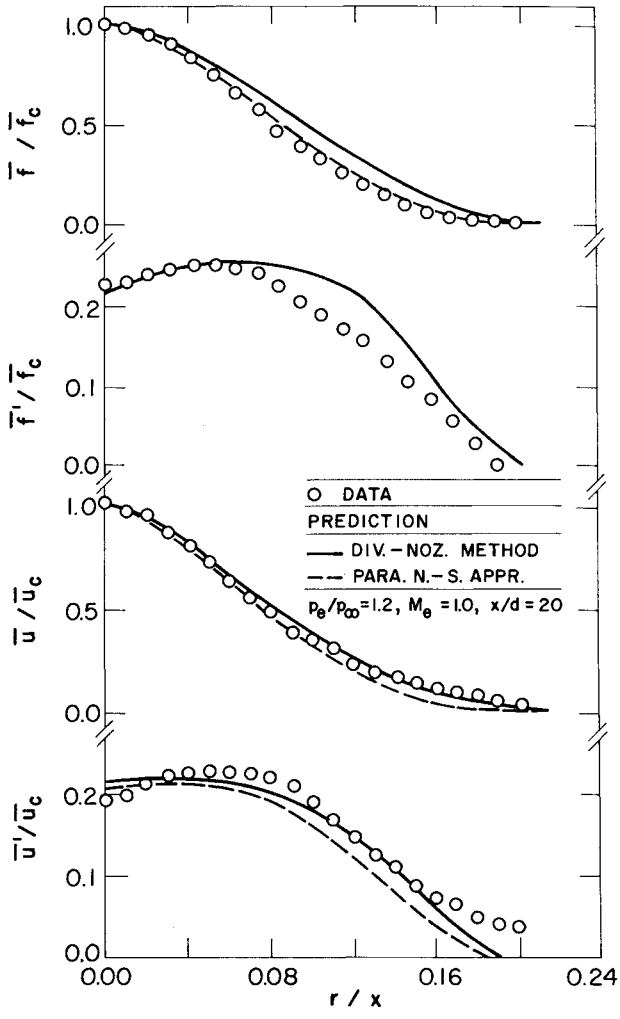

Fig. 10 Mean and fluctuating quantities in an underexpanded jet at $x/d = 20$.

of $x/d = 10$. SCIPVIS predictions of mean properties are also reasonably good, although velocity fluctuations are underestimated due to the problematical assumption of an inviscid core, instead of the turbulent core appropriate for the present measurements.

Conclusions

The major conclusions of the present study are as follows:

1) The shock-wave-containing near-field region of underexpanded turbulent jets is influenced by effects of compressibility (for convective Mach numbers greater than 0.5) and turbulence levels at the jet exit. Compressibility effects reduce turbulent mixing rates for convective Mach numbers greater than 0.5, as described by Bogdanoff[18] and Papamoschou and Roshko,[19] which increases the length of the shock-wave-containing region. Conversely, high turbulence levels at the jet exit increase turbulent mixing rates, similar to subsonic jets, which reduces the length of the shock-wave-containing region. These combined effects represent a formidable problem that must be resolved in order to better understand underexpanded jets for conditions other than weakly underexpanded sonic jets having low turbulence intensity slug flows at the jet exit.

2) Use of the divergent nozzle approximation in conjunction with the compressibility-corrected k-ϵ turbulence model was reasonably successful for estimating the structure of the constant-pressure portions of underexpanded jets (for both fully developed and slug flow jet exit conditions). Unfortunately, this approach provides no information concerning the near-field shock-wave-containing region of the flow.

3) The parabolized Navier-Stokes approach, using the SCIPVIS algorithm and the compressibility-corrected turbulence model, was reasonably successful for slug flows at the jet exit. Additional development of this approach is needed so that effects of turbulence at the jet exit, which are important for some applications, can be accommodated.

4) The present compressibility-correction yielded encouraging results; however, they are provisional, and only limited data were available to calibrate the approach. Additional measurements involving high convective Mach numbers are needed for a more definitive evaluation.

Acknowledgments

This research was supported by the Office of Naval Research, Contract N00014-85-K-0604, with K. Ellingsworth, G. D. Roy, L. A. Parnell, and R. S. Miller serving as Scientific Program Officers.

References

[1]Adamson, T. C., Jr. and Nicholls, J. A., "On the Structure of Jets from Highly Underexpanded Nozzles into Still Air," *Journal of the Aeronautical Sciences*, Vol. 26, Jan. 1959, pp. 16–24.

[2]Crist, S., Sherman, P. M., and Glass, D. R., "Study of the Highly Underexpanded Sonic Jet," *AIAA Journal*, Vol. 4, Jan. 1966, pp. 68–71.

[3]Davidor, W. and Penner, S. S., "Shock Standoff Distances and Mach-Disk Diameters in Underexpanded Sonic Jets," *AIAA Journal*, Vol. 9, Aug. 1971, pp. 1651–1653.

[4]Addy, A. L., "Effects of Axisymmetric Sonic Nozzle Geometry on Mach Disk Characteristics," *AIAA Journal*, Vol. 19, Jan. 1981, pp. 121–122.

[5]Ewan, B. C. R. and Moodie, K., "Structure and Velocity Measurements in Underexpanded Jets," *Combustion Science and Technology*, Vol. 45, March 1986, pp. 275–288.

[6]Seiner, J. M. and Norum, T. D., "Experiments of Shock Associated Noise on Supersonic Jets," AIAA Paper 79-1526, July 1979.

[7]Seiner, J. M. and Norum, T. D., "Aerodynamic Aspects of Shock Containing Jet Plumes," AIAA Paper 80-0965, June 1980.

[8]Birch, A. D., Brown, D. R., Dodson, M. G., and Swaffield, F., "The Structure and Concentration Decay of High Pressure Jets of Natural Gas," *Combustion Science and Technology*, Vol. 36, April 1984, pp. 249–261.

[9]Birch, A. D., Hughes, D. J., and Swaffield, F., "Velocity Decay of High Pressure Jets," *Combustion Science and Technology*, Vol. 52, March 1987, pp. 161–171.

[10]Vatsa, V. N., Werle, M. J., and Anderson, O. L., "Solution of Slightly Underexpanded Two-Dimensional and Axisymmetric Coflowing Jets," *AIAA Journal*, Vol. 19, March 1981, pp. 303–310.

[11]Dash, S. M. and Wolf, D. E., "Interactive Phenomena in Supersonic Jet Mixing Problems, Part I: Phenomenology and Numerical Modeling Techniques," *AIAA Journal*, Vol. 22, Oct. 1984, pp. 905–913.

[12]Dash, S. M., Wolf, D. E., and Seiner, J. M., "Analysis of Turbulent Underexpanded Jets, Part I: Parabolized Navier-Stokes Model, SCIPVIS," *AIAA Journal*, Vol. 23, April 1985, pp. 505–514.

[13]Seiner, J. M., Dash, S. M., and Wolf, D. E., "Analysis of Turbulent Underexpanded Jets, Part II: Shock Noise Features Using SCIPVIS," *AIAA Journal*, Vol. 23, May 1985, pp. 669–677.

[14]Launder, B. E., Morse, A., Rodi, W., and Spalding, D. B., "Prediction of Free Shear Flows: A Comparison of Six Turbulence Models," *Free Turbulent Shear Flows*, Vol. 1, NASA SP-321, 1972, pp. 361–426.

[15]Dash, S. M., Weilerstein, G., and Vaglio-Laurin, R., "Compressibility Effects in Free Turbulence Shear Flows," U.S. Air Force Office of Scientific Research, Washington, DC, AFOSR-TR-75-1436, 1975.

[16]Spalding, D. B., "Concentration Fluctuations in a Round Turbulent Free Jet," *Chemical Engineering Science*, Vol. 26, Jan. 1971, pp. 95–107.

[17]Eggers, J. M., "Velocity Profiles and Eddy Viscosity Distributions Downstream of a Mach 2.2 Nozzle Exhausting to Quiescent Air," NASA TN D-3601, 1966.

[18]Bogdanoff, D. W., "Compressibility Effects in Turbulent Shear Layers," *AIAA Journal*, Vol. 21, June 1983, pp. 926–927.

[19]Papamoschou, D. and Roshko, A., "Observations of Supersonic Free Shear Layers," AIAA Paper 86-0162, Jan. 1986.

[20]Kerney, P. J., Faeth, G. M., and Olson, D. R., "Penetration Characteristics of a Submerged Steam Jet," *AIChE Journal*, Vol. 18, May 1972, pp. 548–553.

[21]Kalghati, G. T., "Blow-Out Stability of Gaseous Jet Diffusion Flames, Part I: In Still Air," *Combustion Science and Technology*, Vol. 26, Oct. 1981, pp. 233-239.

[22]Gore, J. P., Faeth, G. M., Evans, D.,and Pfenning, D. B., "Structure and Radiation Properties of Large-Scale Natural Gas/Air Diffusion Flames," *Fire and Materials*, Vol. 10, 1986, pp. 161-169.

[23]Jeng, S.-M. and Faeth, G. M., "Species Concentrations and Turbulence Properties in Buoyant Methane Diffusion Flames," *Journal of Heat Transfer*, Vol. 106, Nov. 1984, pp. 721-727.

[24]Shuen, J.-S., Solomon, A. S. P., Zhang, Q.-F., and Faeth, G. M., "Structure of Particle-Laden Jets: Measurements and Predictions," *AIAA Journal*, Vol. 23, March 1984, pp. 396-404.

[25]Birch, A. D., Brown, D. R., Dodson, M. G., and Tomason, J. R., "The Turbulent Concentration Field of a Methane Jet," *Journal of Fluid Mechanics*, Vol. 88, Oct. 1978, pp. 431-449.

[26]Becker, H. A., Hottel, H. C., and Williams, G. C., "The Nozzle-Fluid Concentration Field of the Round, Turbulent, Free Jet," *Journal of Fluid Mechanics*, Vol. 30, Nov. 1967, pp. 285-303.

[27]Wygnanski, I. and Fiedler, H., "Some Measurements in the Self-Preserving Jet," *Journal of Fluid Mechanics*, Vol. 38, Sept. 1969, pp. 577-612.

[28]Chuech, S. G., "Kinematic and Scalar Structure of Turbulent Underexpanded Sonic Jets," Ph.D. Thesis, Pennsylvania State University, University Park, PA, 1987.

[29]Lai, M.-C. and Faeth, G. M., "A Combined Laser-Doppler Anemometer/Laser-Induced Fluorescence System for Turbulent Transport Measurements," *Journal of Heat Transfer*, Vol. 109, Feb. 1987, pp. 254-256.

[30]McDaniel, J. C., "Investigation of Laser-Induced Fluorescence for the Measurement of Density in Compressible Flows," Ph.D. Thesis, Stanford University, Stanford, CA, 1983.

[31]Spalding, D. B., *GENMIX: A General Computer Program for Two-Dimensional Parabolic Phenomena*, Pergamon, Oxford, England, 1977.

[32]Maydew, R. C. and Reed, J. F., "Turbulent Mixing of Compressible Free Jets," *AIAA Journal*, Vol. 1, June 1963, pp. 1443-1444.

[33]Sirieux, M. and Solignac, J.-L., "Contribution a l'Etude Experimentale de la Couche de Melange Turbulent Isobare d'un Ecoulement Supersonique," *Symposium on Separated Flow*, AGARD Conference Proceedings, No. 4, Pt. 1, May 1966, pp. 241-270.

[34]Birch, S. F. and Eggers, J. M., "A Critical Review of the Experimental Data for Developed Free Turbulence Shear Layers," *Free Turbulent Shear Flows*, Vol. 2, NASA SP-321, 1972, pp. 11-40.

[35]Brown, G. L. and Roshko, A., "On Density Effects and Large Structures in Turbulent Mixing Layers," *Journal of Fluid Mechanics*, Vol. 64, Pt. 4, 1974, pp. 775-816.

[36]Ikawa, H. and Kubota, T., "Investigation of a Supersonic Turbulent Mixing Layer with Zero Pressure Gradient," *AIAA Journal*, Vol. 13, May 1975, pp. 566-572.

[37]Schlichting, H., *Boundary Layer Theory*, McGraw-Hill, New York, 1979, p. 599.

[38]Hinze, J. O., *Turbulence*, 2nd ed., McGraw-Hill, New York, 1975, pp. 286-300, pp. 715-742.